TU Delft

Delft University of Technology

Document Version
Final published version

Licence
CC BY

Citation (APA)
van der Valk, L. D., Hartogensis, O. K., Coenders-Gerrits, M., Hut, R. W., & Uijlenhoet, R. (2025). Evaporation measurements using commercial microwave links as scintillometers. *Hydrology and Earth System Sciences*, *29*(22), 6589–6606. https://doi.org/10.5194/hess-29-6589-2025

Important note
To cite this publication, please use the final published version (if applicable).
Please check the document version above.

Copyright
In case the licence states “Dutch Copyright Act (Article 25fa)”, this publication was made available Green Open Access via the TU Delft Institutional Repository pursuant to Dutch Copyright Act (Article 25fa, the Taverne amendment). This provision does not affect copyright ownership.
Unless copyright is transferred by contract or statute, it remains with the copyright holder.

Sharing and reuse
Other than for strictly personal use, it is not permitted to download, forward or distribute the text or part of it, without the consent of the author(s) and/or copyright holder(s), unless the work is under an open content license such as Creative Commons.

Takedown policy
Please contact us and provide details if you believe this document breaches copyrights.
We will remove access to the work immediately and investigate your claim.

This work is downloaded from Delft University of Technology.

Hydrol. Earth Syst. Sci., 29, 6589–6606, 2025
https://doi.org/10.5194/hess-29-6589-2025
© Author(s) 2025. This work is distributed under
the Creative Commons Attribution 4.0 License.

Hydrology and Earth System Sciences
Open Access
EGU

Evaporation measurements using commercial microwave links as scintillometers

Luuk D. van der Valk[1], **Oscar K. Hartogensis**[2], **Miriam Coenders-Gerrits**[1], **Rolf W. Hut**[1], **and Remko Uijlenhoet**[1]

[1]Department of Water Management, Delft University of Technology, Delft, the Netherlands
[2]Meteorology and Air Quality Group, Wageningen University & Research, Wageningen, the Netherlands

Correspondence: Luuk D. van der Valk (l.d.vandervalk@tudelft.nl)

Received: 10 March 2025 – Discussion started: 5 May 2025
Revised: 9 July 2025 – Accepted: 5 September 2025 – Published: 21 November 2025

Abstract. As the spatial coverage of evaporation observations is limited, we propose a novel, opportunistic method to estimate evaporation in which we consider commercial microwave links (CMLs), such as used in cellular telecommunication networks, in combination with scintillometry. Scintillometers are dedicated instruments to measure path-integrated latent and sensible heat fluxes, transmitting electromagnetic radiation that is diffracted by turbulent eddies between transmitter and receiver, causing the so-called scintillation effect. CMLs are line-of-sight devices that transmit electromagnetic radiation at similar frequencies as microwave scintillometers. However, CMLs and their sampling strategies are designed to ensure a continuously functioning wireless communication network rather than to capture the scintillation effect. Here, we estimate 30 min latent heat fluxes and daily evaporation using a former CML. To do so, we use data of a 38 GHz Nokia CML (formerly part of a telecom network) installed over an 856 m path at the Ruisdael Observatory near Cabauw, the Netherlands. We compare our results with estimates from an optical and microwave scintillometer setup, as well as an EC system. To obtain the flux estimates using the CML, we apply the two-wavelength method, in combination with the optical scintillometer, as well as a standalone energy-balance method (EBM), requiring net radiation estimates. For comparison, we also consider the free-convection limit of Monin-Obukhov similarity theory (MOST), instead of the complete scaling. An advantage of this approach is that it does not require horizontal wind speed measurements, which are more difficult to obtain in complex environments. For the net radiation estimates, we use in-situ measured radiation and data products provided by the Satellite Application Facility on Land Surface Analysis (LSA SAF) of EUMETSAT. Considering both turbulent heat fluxes, the two-wavelength method outperforms the EBM. The standalone EBM shows a reasonable performance, but also a large dependence on the quality of the net radiation estimates. When aggregating our 30 min latent heat fluxes to daily evaporation estimates, the relative performance of the methods remains comparable to that at 30 min intervals. These daily evaporation estimates could also be useful for catchment hydrological applications. Application of the free-convection scaling instead of the complete MOST scaling results in a comparable performance for all methods.

1 Introduction

Evaporation plays a key role in the energy and water cycle, yet large-scale evaporation observations are not readily available. Global coverage of in-situ networks, e.g., consisting of eddy-covariance (EC) systems, like FLUXNET, is relatively low and cannot represent all ecosystems and continents (e.g., Villarreal and Vargas, 2021; Pallandt et al., 2022). In comparison, satellite remote sensing estimates of evaporation have a better spatial coverage, but have a low temporal and limited spatial resolution (Zhang et al., 2016). Also, the method relies on indirect relations between surface characteristics and evaporation, while also clouds can be a limiting factor. As an alternative to these methods, Leijnse et al. (2007b) proposed using commercial microwave links (CMLs), which are near-surface terrestrial radio connections used in cellular telecommunication networks, as scintillometers to obtain latent and sensible heat flux estimates.

To measure evaporation, CMLs can be used in combination with scintillation theory, which derives turbulent characteristics of the atmosphere from fluctuations in the received signal intensity, so-called scintillations (e.g., Ward, 2017). The frequencies of the transmitted electromagnetic radiation by CMLs are comparable to those employed by microwave scintillometers, which are dedicated instruments to obtain the surface turbulent heat fluxes (e.g., Kohsiek, 1982; Green et al., 2001; Ward et al., 2015b). As the transmitted scintillometer signal propagates through the atmosphere, turbulent eddies scatter the beam, so that at the receiving end the signal intensity fluctuates. The scattering properties of the atmosphere, expressed as the structure parameter of the refractive index C_{nn}, depend on the frequency of the transmitted signal and density of these eddies, which is affected by temperature and humidity of these eddies. To separate the signal intensity fluctuations into temperature and humidity induced fluctuations, usually a two-wavelength scintillometer setup is used. This typically includes a microwave scintillometer (MWS), of which the signal is affected by both temperature and humidity fluctuations, and an optical scintillometer, of which the signal is mostly affected by temperature fluctuations. These separated fluctuations in temperature and humidity can be related to the surface turbulent heat fluxes using Monin-Obukhov similarity theory (Monin and Obukhov, 1954).

As an advantage, CML networks have a large spatial coverage, also at locations where in-situ observation networks are absent, and are actively maintained by mobile network operators. It is estimated that 6 million CMLs will be operationally employed in 2027 (ABI research, 2021). Moreover, CMLs are already used to measure path-averaged rainfall (e.g., Messer et al., 2006; Leijnse et al., 2007a), so that theoretically these networks could be used to measure both water fluxes between the atmosphere and land surface. However, using CMLs as scintillometers also introduces challenges, such as noise floors in antennas, power quantization (i.e., discretization of the signal intensity) and typical temporal sampling strategies in CML network management systems at relatively coarse temporal resolutions, i.e., ~ 15 min (van der Valk et al., 2025a).

In this study, we build on the results of van der Valk et al. (2025a), where we aimed to obtain the best possible 30 min C_{nn} estimates using a CML formerly employed in a telecommunication network in the Netherlands. We found that the CML, an 38 GHz Nokia CML sampled at 20 Hz, adds white noise to the signal intensity, resulting in an overestimation of C_{nn} values. In order to correct for that, we proposed two methods. The first method applies a high-pass filter and subtracts a low quantile of the resulting variances of the Nokia CML, called the constant noise correction method. The second method corrects for the noise in the Nokia CML by comparing with an MWS and selecting parts of the power spectra where the Nokia Flexihopper behaves in correspondence with scintillation theory, called the spectral noise correction method. The latter method also considers different crosswind conditions and corrects for the omitted scintillations using scintillation theory. Both correction methods showed a major improvement in comparison to the uncorrected C_{nn} estimates. The spectral noise method outperformed the constant noise method, mostly by reducing the spread compared to the reference instruments, the MWS and an EC system. An advantage of the constant noise method is that it provides a straightforward correction, without the need for a collocated MWS. However, it is unclear what the effect of the uncertainty in these C_{nn} estimates on the eventual turbulent heat fluxes is. The aim of this study is to obtain latent heat fluxes using the proposed correction methods of van der Valk et al. (2025a).

Here, we focus on obtaining 30 min latent heat flux and daily evaporation estimates from the Nokia CML using the scintillometer method. To do so, we use the same Nokia CML as van der Valk et al. (2025a), which is installed at the Ruisdael Observatory near Cabauw, the Netherlands, and examine data between 1 April and 1 October 2024, corresponding to a full growing season in the Netherlands. We try to obtain flux estimates with the CML using the regular two-wavelength method, in which a microwave scintillometer is combined with an optical scintillometer. Moreover, we explore a standalone method based on the energy balance (as proposed by Leijnse et al., 2007b), which can be used to obtain the latent heat fluxes by combining the C_{nn} estimates with more widely available input data than an optical scintillometer. Additionally, to reduce the number of required meteorological observations, we consider the free-convection limit of Monin-Obukhov similarity theory, instead of the complete scaling. We elaborate on these methods in Sect. 2. We compare our latent heat flux estimates with a two-wavelength scintillometer setup (microwave and optical) and an EC setup. Overall, this setup allows us to investigate the potential of CMLs to estimate 30 min latent heat fluxes and daily evaporation in well-monitored and relatively idealized conditions.

2 Obtaining the turbulent heat fluxes from C_{nn}

To relate the structure parameter of the refractive index, C_{nn}, to the turbulent heat fluxes, first the structure parameters of temperature, C_{TT}, and humidity, C_{qq}, have to be determined. C_{nn} is affected by C_{TT} [$\mathrm{K^2\,m^{-2/3}}$], C_{qq} [$\mathrm{kg^2\,kg^{-2}\,m^{-2/3}}$] and the cross-structure parameter C_{Tq} [$\mathrm{K\,kg\,kg^{-1}\,m^{-2/3}}$] (e.g., Foken, 2021):

$$C_{nn} = \frac{A_T^2}{\overline{T}^2} C_{TT} + \frac{A_q^2}{\overline{q}^2} C_{qq} + 2\frac{A_T A_q}{\overline{T}\,\overline{q}} C_{Tq}, \tag{1}$$

in which A_T and A_q are the structure parameter coefficients for temperature and specific humidity, respectively (e.g., given in Ward et al., 2013), $\overline{T}$ is the average air temperature [K] and $\overline{q}$ is the average specific humidity [$\mathrm{kg\,kg^{-1}}$].

These coefficients are dependent on temperature, humidity, pressure and the wavelength of the scintillometer.

2.1 Two-wavelength setups

Typically in scintillometer systems, a two-wavelength setup is installed, so that C_{TT} and C_{qq} can be retrieved from the C_{nn} estimates of both scintillometers. Usually, this involves a microwave scintillometer (MWS) and a large-aperture scintillometer (LAS), which operates at optical wavelengths. The C_{nn} estimates obtained from the MWS are affected by both the temperature and humidity fluctuations in Eq. (1), while the C_{nn} estimates obtained from the LAS are dominated by temperature fluctuations. C_{Tq} can be measured by correlating the LAS and MWS signals (called bichromatic method; Lüdi et al., 2005) or estimated by assuming a value for the temperature-humidity correlation coefficient r_{Tq}:

$$C_{Tq} = r_{Tq}\sqrt{C_{TT}C_{qq}}. \tag{2}$$

Typical values for r_{Tq} are around 0.8 for unstable conditions and -0.5 for stable conditions (Ward, 2017). Similar to Ward et al. (2015b), we assume r_{Tq} to be 0.8 for daytime conditions, who find this to be a reasonable value, consistent with values obtained from fast-response sensors (e.g., Kohsiek, 1982; Meijninger et al., 2002).

Subsequently, when using the two-wavelength method, C_{TT} and C_{qq}, can be computed using (e.g., Hill, 1997):

$$\begin{aligned} C_{TT} &= \frac{A_{q2}^2 C_{nn1} + A_{q1}^2 C_{nn2} + 2r_{Tq}A_{q1}A_{q2}S_{2\lambda}\sqrt{C_{nn1}C_{nn2}}}{(A_{T1}A_{q2} - A_{T2}A_{q1})^2 T^{-2}}, \\ C_{qq} &= \frac{A_{T2}^2 C_{nn1} + A_{T1}^2 C_{nn2} + 2r_{Tq}A_{T1}A_{T2}S_{2\lambda}\sqrt{C_{nn1}C_{nn2}}}{(A_{T1}A_{q2} - A_{T2}A_{q1})^2 q^{-2}}, \end{aligned} \tag{3}$$

in which subscripts 1 and 2 refer to the LAS and MWS, respectively, and $S_{2\lambda}$ originates from the two possible solutions for the C_{nn} of microwave signals (Hill, 1997). When humidity fluctuations dominate (i.e., a low Bowen ratio) $S_{2\lambda}$ equals 1, while when temperature fluctuations dominate (i.e., a high Bowen ratio) $S_{2\lambda}$ equals -1. For our study, we assume $S_{2\lambda}$ equals 1, given the relatively wet conditions at our field site (e.g., Brauer et al., 2014).

After obtaining C_{TT} and C_{qq}, these can be related to the turbulent heat fluxes using Monin-Obukhov similarity theory (MOST). First, C_{TT} and C_{qq} are related to the average turbulent temperature $\overline{T}_*$ [K] and humidity scales $\overline{q}_*$ [kg kg^{-1}],

$$\begin{aligned} \frac{C_{TT}z^{2/3}}{\overline{T}_*^2} &= f_{TT}\left(\frac{z-d}{L_{\mathrm{Ob}}}\right), \\ \frac{C_{\mathrm{qq}}z^{2/3}}{\overline{q}_*^2} &= f_{qq}\left(\frac{z-d}{L_{\mathrm{Ob}}}\right), \end{aligned} \tag{4}$$

in which z is the measurement height [m], d is the displacement height [m], L_{Ob} is the Obukhov length [m], and f_{TT} and f_{qq} are universal functions (e.g., Wyngaard et al., 1971b). The turbulent heat fluxes are directly related to T_* and q_*:

$$\begin{aligned} T_* &= -\frac{H}{\overline{\rho}c_{\mathrm{p}}u_*}, \\ q_* &= \frac{(1-\overline{q})L_{\mathrm{v}}E}{\overline{\rho}L_{\mathrm{v}}u_*}, \end{aligned} \tag{5}$$

in which H is the sensible heat flux [W m^{-2}], $L_{\mathrm{v}}E$ is the latent heat flux [W m^{-2}], ρ is the air density [kg m^{-3}], c_{p} is the specific heat capacity of air [J kg^{-1} K^{-1}], u_* is the friction velocity [m s^{-1}] and L_{v} is the latent heat of vaporization [J kg^{-1}].

The f_{TT} and f_{qq} functions usually have the form (for unstable conditions):

$$f\left(\frac{z-d}{L_{\mathrm{Ob}}}\right) = c_1\left(1 - c_2\left(\frac{z-d}{L_{\mathrm{Ob}}}\right)\right)^{-2/3}, \tag{6}$$

in which c_1 and c_2 are constants that differ for f_{TT} and f_{qq} and depend on stability. Kooijmans and Hartogensis (2016) compare measurements from different datasets in order to obtain robust similarity functions including an uncertainty range for these functions. For f_{TT} in unstable conditions, c_1 and c_2 are equal to 5.6 and 6.5, respectively. For f_{qq} in unstable conditions, c_1 and c_2 are equal to 4.5 and 7.3, respectively. L_{Ob} is defined as:

$$L_{\mathrm{Ob}} = -\frac{\overline{\rho}c_{\mathrm{p}}\overline{T}u_*^3}{g\kappa H}, \tag{7}$$

in which g is the gravitational acceleration [m s^{-2}] and κ is the von-Karmán constant. u_* can be calculated using horizontal wind speed measurements U [m s^{-1}]:

$$u_* = \frac{\kappa U}{\log\left(\frac{z_u-d}{z_0}\right) - \psi_M\left(\frac{z_u-d}{L_{\mathrm{Ob}}}\right) + \psi_M\left(\frac{z_0}{L_{\mathrm{Ob}}}\right)}, \tag{8}$$

in which z_u is the measurement height of U [m], z_0 is the roughness length for momentum [m] and ψ_M is the Businger-Dyer expression (e.g., Brutsaert, 1982).

Thus, next to the scintillometer measurements, the two-wavelength method requires temperature, humidity and horizontal wind speed measurements. Additionally, it requires more complex measurements of the correlation between temperature and humidity fluctuations, the roughness length for momentum and the displacement height. For the roughness length z_0, we make use of values reported by Moonen (2021), who determined the roughness length for various wind sectors using EC data (Table 1) and found similar values to Verkaik and Holtslag (2007). For the displacement height d, we use the relationship $d = \frac{16}{3}z_0$ from Brutsaert (1982).

In order to obtain the turbulent heat fluxes, Eqs. (4)–(7) have to be solved iteratively. In figures, we refer to the two-wavelength method using the suffix 2λ. We refer the reader to Appendix A for a complete overview of the used abbreviations.

Table 1. Lower and upper bound of wind direction classes and roughness length z_0 values as determined by Moonen (2021).

Lower bound [°]	Upper bound [°]	z_0 [m]
40	100	0.03
100	160	0.01
160	280	0.005
280	40	0.01

2.2 Standalone methods

To compute the turbulent heat fluxes using CMLs, a LAS is usually not available, so that standalone methods need to be defined. These standalone methods require an additional constraint or assumption in order to separate C_{nn} into C_{TT} and C_{qq}, and subsequently into the turbulent heat fluxes. In this study, we use the energy balance as constraint, hereafter referred to as EBM (Leijnse et al., 2007b). To do so, closure of the measured energy balance is assumed:

$$R_{\text{net}} - G = L_{\text{v}}E + H, \tag{9}$$

in which R_{net} is the net radiation [W m^{-2}] and G is the ground heat flux [W m^{-2}]. In combination with Eqs. (1), (4)–(8), both the turbulent heat fluxes can be solved iteratively. In this study, we apply this method using in-situ measurements and LSA SAF data products to obtain the net radiation (Sect. 3.3). For the in-situ method, we use the measured ground heat flux, while for the remotely sensed data product we assume 10 % of the net radiation is used for the ground heat flux. Note that the measured energy balance hardly ever closes, especially in more complex measurement environments, e.g., forests or cities (Mauder et al., 2020). For the field site used in this study, Cabauw in the Netherlands, typically an imbalance during day-time is found between 10 % (afternoons) to 40 % (mornings) (Kroon, 2004). For our data period we find similar values using EC data (not shown).

As alternative constraint, we considered prescribing a Bowen ratio instead of net radiation, however that did not yield promising results. We applied the Bowen ratio obtained from the estimated turbulent heat fluxes by LSA SAF. An advantage is that this does not require radiation estimates, but the performance depends largely on the quality of the prescribed Bowen ratio. In the remainder of this article, we refer to the EBM using in-situ radiation data with EBM-OBS, and for the method using the LSA data products, we use EBM-LSA. We refer the reader to Appendix A for a complete overview of the used abbreviations.

2.3 Free-convection scaling

Free-convection scaling can be applied to further reduce the number of required meteorological observations, as no horizontal wind speed measurements are necessary. This scaling assumes the turbulent heat fluxes are solely a result of convection. A disadvantage of this assumption is that it introduces an underestimation of the turbulent heat fluxes in comparison to the complete scaling, which also includes wind shear as source of the fluxes. However, this underestimation is relatively little as, using the method of De Bruin et al. (1995) to estimate the underestimation of free-convection, we find that $L_{\text{v}}E$ is underestimated less than 5 % for $-\frac{z-d}{L_{\text{Ob}}}$ values larger than 1 (Fig. 1). An advantage of CMLs is that they are typically mounted relatively high above the ground surface (at least 20–30 m), especially in comparison to typical scintillometer heights, so that $-\frac{z-d}{L_{\text{Ob}}}$ also is relatively large with constant L_{Ob}.

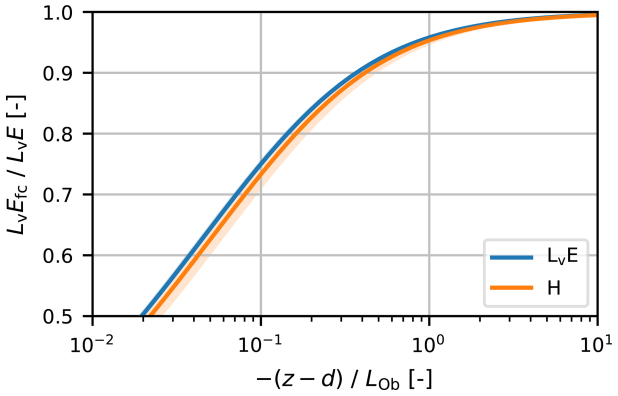


Figure 1. Underestimation of the free-convection scaling versus the complete scaling as function of $-\frac{z-d}{L_{\text{Ob}}}$. The bands indicate the uncertainty based on the uncertainty estimates of the MOST universal functions coefficients by Kooijmans and Hartogensis (2016). For $L_{\text{v}}E$ this uncertainty band is relatively small in comparison to H.

For free-convection scaling, C_{TT} and C_{qq} in Eq. (4) are not scaled with T_* and q_*, but with T_{fc} and q_{fc}, which are defined as (Wyngaard et al., 1971a):

$$T_{\text{fc}} = \frac{H}{\overline{\rho} c_p u_{\text{fc}}},$$
$$q_{\text{fc}} = \frac{L_{\text{v}}E}{\overline{\rho} L_{\text{v}} u_{\text{fc}}}, \tag{10}$$

in which u_{fc} is the scaling wind velocity [m s^{-1}], defined as:

$$u_{\text{fc}} = \left(\frac{g(z-d)}{T}\frac{H}{\rho c_p}\right)^{1/3}. \tag{11}$$

Finally, replacing T_* and q_* in Eq. (4) with T_{fc} and q_{fc} and assuming $-\left(\frac{z}{L_{\text{Ob}}}\right)$ goes to infinity, results in Kohsiek (1982):

$$H = \pm a\rho c_{\text{p}}(z-d)\left(\frac{g}{T}\right)^{1/2} C_{TT}^{3/4},$$
$$L_{\text{v}}E = \pm b\rho L_{\text{v}}(z-d)\left(\frac{g}{T}\right)^{1/2} C_{TT}^{1/4} C_{qq}^{1/2}, \tag{12}$$

in which a and b are empirical constants based on the universal function (Eq. 6), which are 0.44 and 0.51 respec-

tively, using the values reported by Kooijmans and Hartogensis (2016). Using their reported uncertainty of these coefficients, a ranges between 0.37 and 0.51, and b between 0.47 and 0.56. In Sect. 4, we apply the complete and free-convection scaling for all our methods, and refer to the latter in the figures with suffix FC. We refer the reader to Appendix A for a complete overview of the used abbreviations.

3 Instrument and data description

3.1 Experimental setup

We use the same experimental setup as van der Valk et al. (2025a). This experiment is conducted at the Ruisdael Observatory at Cabauw, the Netherlands. We installed a commercial microwave links collocated to a MWS and LAS setup over an 856 m path between 51.974252° N, 4.923484° E and 51.967552° N, 4.929561° E (Fig. 2). The CML and scintillometers are installed on a 10 m high, vibration-free mast. We use daytime data from from 1 April to 1 October 2024, which corresponds to a growing season in the Netherlands. Moreover, it is important to note that management of the water table aims to have a constant soil water content in the rootzone, approximately at field capacity (e.g., Brauer et al., 2014). The dominant wind direction at Cabauw is southwesterly, so that the footprints of the scintillometers and EC mostly consist of grass fields. Only for northerly wind directions built-up area may partly be included.

3.2 Measurement equipment

The CML used in this study is a Nokia Flexihopper, formerly employed in a commercial mobile phone network operated by T-Mobile Netherlands (currently, Odido Netherlands). This link is mounted at 10 m above the surface and transmits at 38.1745 GHz with a bandwidth of 0.9 MHz. The signal intensity is sampled at 20 Hz. In van der Valk et al. (2025a), it is shown that the signal of this CML contains added white noise. Therefore, we suggest two C_{nn} correction methods, a constant noise correction method, which is a more generic correction, and a spectral noise correction method. Even though the constant noise method is outperformed by the spectral noise method, we show results of both methods in our current analysis, because the constant noise method is a straightforward correction method, which can be applied without a comparison with an MWS.

As reference instruments, we use an optical-microwave scintillometer setup and an eddy-covariance system (EC). The scintillometer setup consists of a Radiometer Physics RPG-MWSC-160 microwave scintillometer, transmitting at 160.8 GHz (i.e., a wavelength of 1.86 mm), and a Kipp & Zonen LAS Mk-II, transmitting at 352.7 THz (i.e., a wavelength of 850 nm), which are both sampled at 1 kHz. Hereafter we refer to this system as MWS-2λ. The path of this scintillometer setup is nearly identical to the path of the CML (e.g., Fig. 2), so that differences in footprints can be neglected. It should be noted that this setup has a major data gap between 10 July and 6 September 2024. The EC system consists of a sonic anemometer (Gill-R50) and an open-path H_2O / CO_2 sensor (LICOR-7500), sampled at 10 Hz, and installed at 3 m above the ground (Bosveld et al., 2020). The fluxes obtained with the EC can directly obtained from the KNMI Data Platform (2024), next to other more common meteorological measurements. The EC data is available during the entire study period. During the dominant southwesterly wind direction, the footprints of the EC, scintillometer setup and CML all predominantly consist of grass fields.

After computing 30 min L_vE estimates, we perform our analysis based on 30 min L_vE [W m^{-2}] and daily E [mm d^{-1}] estimates. The former is a typical time interval for turbulent heat flux research (e.g., Green et al., 2001; Meijninger et al., 2002), while the latter time scales are more commonly used in hydrological applications. In order to be able to compare daily E estimates, we only aggregate the 30 min time intervals per day that are available for both the Nokia CML and the reference instrument.

In our analysis, we remove nighttime intervals and intervals with high absolute wind speeds. We assume incoming shortwave radiation above 20 W m^{-2} to exclude nighttime intervals, during which negligible evaporation takes place. As threshold for absolute wind speeds we use 8 m s^{-1}, because the Nokia CML vibrates during higher wind speeds (van der Valk et al., 2025a). This is caused by the relatively weak mounting system of the Nokia, as no vibrations are found in MWS even though both are mounted in the same mast. Additionally, we remove rainy intervals or those following a rain event within an hour, in order to exclude the effects of wet-antenna attenuation.

3.3 Remotely-sensed net radiation estimates

For the method of Leijnse et al. (2007b), net radiation measurements are required. To overcome the lacking availability of these measurements for CML networks, we consider the radiation products of Satellite Application Facility on Land Surface Analysis (LSA SAF) of EUMETSAT (EUMETSAT, 2025). Similar to Rains et al. (2024), we use the 15 min incoming shortwave radiation $SW_\downarrow$ [W m^{-2}], 30 min incoming longwave radiation $LW_\downarrow$ [W m^{-2}], daily albedo α, daily emissivity ϵ and 30 min land surface temperature T_{surf} [K] products to compute 30 min net radiation estimates using:

$$R_{net} = SW_\downarrow + LW_\downarrow - \alpha SW_\downarrow - (\epsilon\sigma T_{surf}^4 + (1-\epsilon)LW_\downarrow), \quad (13)$$

in which σ is the Stefan-Boltzmann constant (i.e., 5.67×10^{-8} W m^{-2} K^{-4}). In order to obtain 30 min net radiation estimates, we average $SW_\downarrow$ to 30 min time intervals and assume α and ϵ are constant for the full day. Note that $(1-\epsilon)LW_\downarrow$ in the outgoing longwave radiation term originates from long-wave reflection (e.g., Maes and Steppe, 2012). Rains et al. (2024) show that hourly net radiation

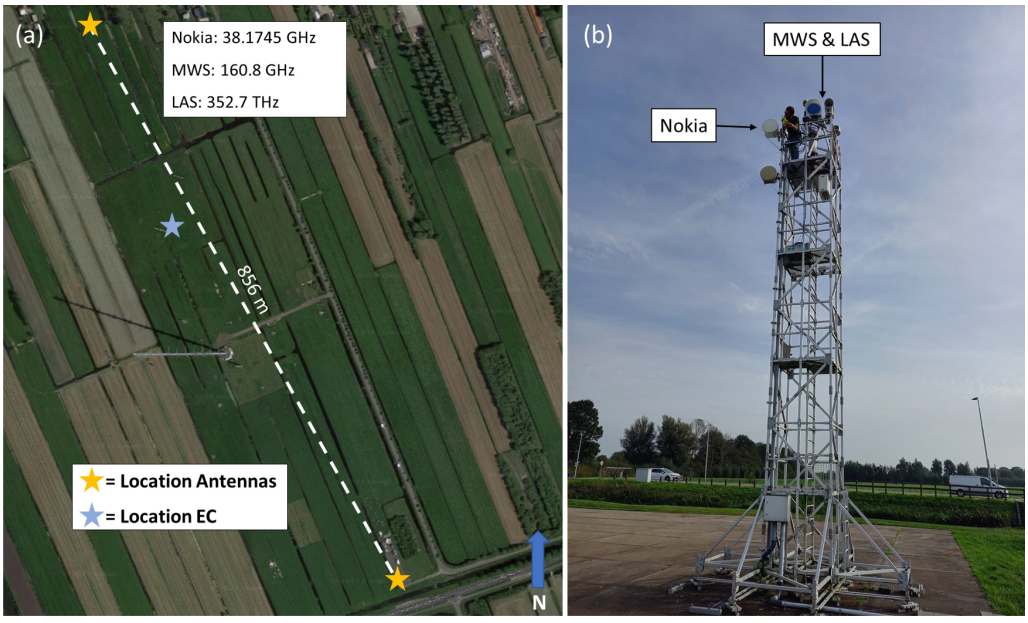


Figure 2. (a) Overview of (formerly employed) Nokia CML, MWS, LAS and EC at the Ruisdael Observatory, Cabauw. Reported frequencies are the transmitting frequencies per antenna. **(b)** The southern mast with 3 installed instruments. From top to bottom: the receivers of the MWS and LAS, the Nokia Flexihopper and an Ericsson MiniLink (not used in this study). Figure is based on van der Valk et al. (2025a) (© Google Maps).

obtained with LSA SAF performs generally comparable to other large-scale products, e.g., the ERA5-Land product, and has on average a root mean square error of 23.5 $\mathrm{W\,m^{-2}}$, an average bias of $-9\,\mathrm{W\,m^{-2}}$ and a correlation coefficient of 0.93 when comparing to in-situ data over Europe. For Cabauw during our data period, the net radiation obtained with LSA SAF compared to the measured net radiation on average shows similar error estimates, though with an overestimation (Fig. B1).

3.4 Error estimates

In this study, we compare 30 min $L_\mathrm{v}E$ estimates and daily E estimates [$\mathrm{mm\,d^{-1}}$]. In all comparisons, we use the mean bias error (MBE), the 10–90 interquantile range (IQR) and Pearson's correlation coefficient (r). The MBE and IQR are calculated as:

$$\begin{aligned} \mathrm{MBE} &= \overline{y - x}, \\ \mathrm{IQR} &= P_{90} - P_{10}, \end{aligned} \tag{14}$$

in which y are the $L_\mathrm{v}E$ or E estimates of the instrument on the y-axis and x are the $L_\mathrm{v}E$ and E estimates of the instrument on the x-axis, i.e., the reference MWS-2λ or EC system. Similarly, P_{90} and P_{10} are the 90th and 10th percentiles of the difference between the $L_\mathrm{v}E$ or E estimates of the instrument on the y-axis and the $L_\mathrm{v}E$ or E estimates of the instrument on the x-axis of a scatterplot. The units of the MBE and IQR are the same as the variable presented in the scatterplot.

4 Results

4.1 30 min $L_\mathrm{v}E$ estimates

A comparison of the reference methods for the full data period shows an overall comparable behaviour (Fig. 3), indicating negligible influence of differences in footprints between the two references. On average, however, the MWS-2λ method shows an overestimation in comparison to EC. For the monthly median diurnal cycles, all CML methods with the spectral noise correction overestimate $L_\mathrm{v}E$ compared to the references (Fig. 4). This overestimation is roughly constant throughout our data period, with the exception of June, during which the overestimation in comparison to the reference methods is larger. The diurnal cycle is well captured by all CML methods, even when considering the interquartile range. Noteworthy, is the similarity between the CML-2λ and CML-EBM-OBS methods in the diurnal cycles, both in median values and uncertainty. The clearest differences between these methods occur before sunset, when the CML-2λ method overestimates LvE, while the CML-EBM-OBS estimates are constrained by the measured net radiation.

Subsequently, we examine the performance of both corrections (constant and spectral noise), all methods (two-wavelength, EBM-OBS and EBM-LSA) and both scalings (complete and free-convection) in comparison to our reference instruments. Figure 5 shows scatter density plots for both correction methods with the two-wavelength method using the complete scaling. These plots show that the two

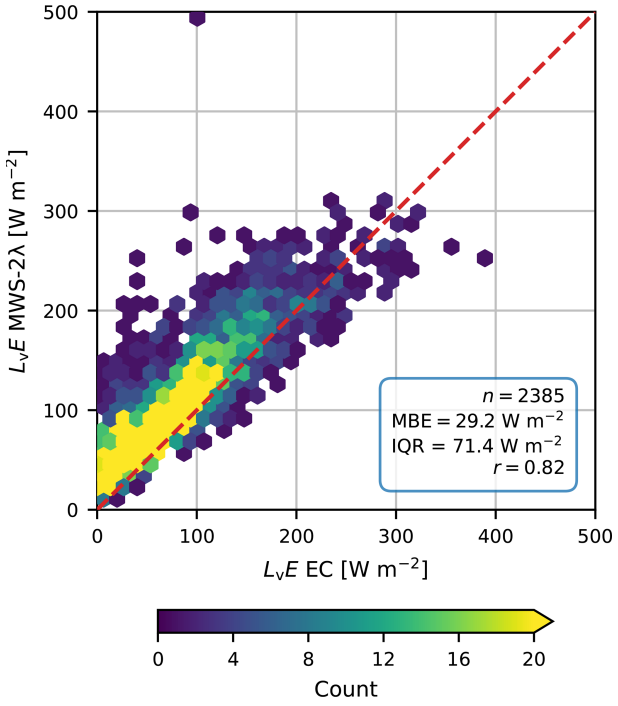


Figure 3. Comparison of 30 min L_vE estimates obtained with the MWS-2λ method versus the EC estimates. MWS-2λ method uses the 2 wavelength scintillation method with the MWS and LAS, and EC are the eddy-covariance estimates. The dashed red line is the 1 : 1 line.

example time series are not fully representative of the overall performance. For example, the typically found overestimation of high L_vE values for CML-2λ are not visible in Fig. 4b. In Fig. 6, we present all statistical metrics for the 30 min L_vE estimates using all possible combinations of corrections, methods and scalings. In this plot, we also show the intercomparison between the reference methods and two comparisons with alternative methods to derive L_vE. These alternatives are the L_vE estimates obtained directly from LSA SAF versus those from the MWS-2λ method and L_vE estimates based on $R_{net} - G$ and a Bowen ratio versus those from the MWS-2λ method. We show these methods to illustrate how a readily available (former) and a basic experimental method from only net radiation estimates (latter) perform in comparison to the reference instruments. The used Bowen ratio is obtained from the EC and is the median ratio for the full data period (excluding nighttime intervals). We use a median value as a means to obtain an objectively selected, representative Bowen ration value to estimate L_vE from only net radiation measurements. For all the corresponding scatter density plots we refer the reader to the supplementary materials. The statistical plot for H can be found in Appendix C, and the corresponding scatter density plots can also be found in the Supplement.

4.1.1 Energy-balance method versus two-wavelength method

Overall, the EBM-OBS outperforms the other two methods for the L_vE estimates. It has a lower MBE and IQR than the two-wavelength method and the EBM-LSA. All methods have a comparable r in comparison to the MWS-2λ method. We would have expected the two-wavelength method to perform best, as this is closest to the traditional two-wavelength setup, but it has a higher MBE than both the EBM versions. The H estimates of both EBM versions perform less well than the estimates of the two-wavelength method. This is in line with our expectations, because the LAS signal dominates these estimates. (Fig. C1). The H estimates of EBM-OBS have an MBE and IQR similar to the L_vE estimates, even though the L_vE is the highest of the two turbulent heat fluxes at Cabauw. These differences in performance between the turbulent heat fluxes are mostly a consequence of the nature of these methods in combination with the overestimation of C_{nn} by the CML (see van der Valk et al., 2025a). For the two-wavelength method, this overestimation is fully attributed to the L_vE, since H is constrained by the same LAS estimates for the CML-2λ and the MWS-2λ methods, while for the EBM methods this overestimation can be distributed among L_vE and H. Note that the EBM-LSA has a higher MBE and IQR than the EBM-OBS, most likely due to the overestimation and uncertainty of R_{net} by LSA SAF (Fig. B1).

4.1.2 C_{nn} Correction methods

For both correction methods, the MBE results are approximately equal, while the IQR and r improve for the spectral noise method, similar to the findings of van der Valk et al. (2025a). They argue that this can be attributed to the nature of the correction method. The constant noise correction method is relatively basic and subtracts a constant value of all C_{nn} values. The spectral noise correction method selects the best performing parts of the power spectra, which reduces the overall spread of the C_{nn}, and thus L_vE, estimates.

4.1.3 Free Convection scaling

For the two-wavelength method, the free-convection scaling behaves as described in Sect. 2.3, with a reduction in turbulent heat fluxes in comparison to the complete scaling. Overall, this improves the statistical metrics of the L_vE estimates of the two-wavelength method, although for the wrong reasons (i.e., neglecting shear-driven turbulence). For both EBM versions, the L_vE estimates using free-convection scaling increase in comparison to the complete scaling, while the H estimates decrease, as a result of the available energy $R_{net} - G$ being distributed among L_vE and H.

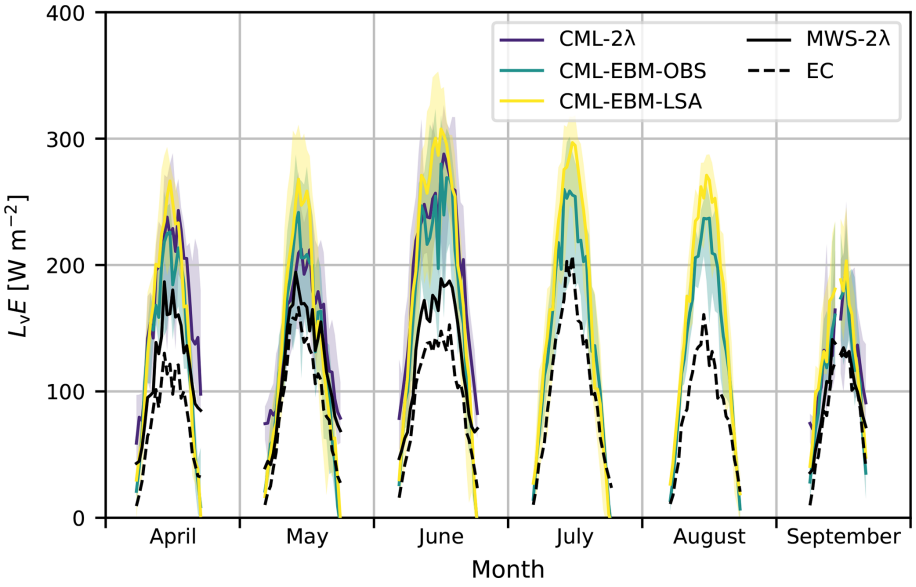


Figure 4. Median diurnal cycles and interquartile ranges (shading) of 30 min L_vE estimates of the methods for the Nokia CML in comparison with the reference instruments. CML-2λ method uses the two-wavelength scintillation method with the CML and LAS, CML-EBM-OBS uses the measured energy balance method as constraint to infer the turbulent heat fluxes and CML-EBM-LSA uses the estimated net radiation by LSA SAF instead of the measured net radiation. Shown estimates are obtained using the spectral noise method for the CML estimates and complete Monin-Obukhov scaling. We removed timestamps with less than 10 available days in order to obtain representative diurnal cycles. We refer the reader to Appendix A for a complete overview of the used abbreviations.

4.1.4 Comparison with alternative L_vE methods

A comparison with two alternative methods to retrieve L_vE estimates shows that estimating L_vE using CMLs can be beneficial, especially regarding the spread. One of these alternative methods is based on the measured energy balance and prescribing a median Bowen ratio based on the EC data, i.e., the best possible estimation of the Bowen ratio, results in higher IQR in comparison to the MWS-2λ method than any of the methods using the CML. The other alternative is the L_vE estimates obtained from LSA SAF data product. A comparison between these LSA SAF L_vE estimates versus the MWS-2λ method is also outperformed on the IQR by the majority of the methods using the CML. In comparison to this method, it should be noted that the EBM-LSA only shows a minor improvement.

4.2 Daily E estimates

In comparison to the 30 min L_vE estimates, the daily E estimates show a similar behaviour (Fig. 7). The spread found in the 30 min L_vE estimates (Fig. 5) is also found for the daily time intervals. Thus, it seems that the occurrence of outliers is not related to specific atmospheric conditions, illustrating the robustness of the methods. Overall, this makes that the patterns in the daily statistics are comparable to the 30 min statistics when aggregating the 30 min estimates to daily intervals (Fig. 8).

5 Discussion

This study aims to obtain L_vE estimates using CMLs as scintillometers and builds on the correction methods proposed by van der Valk et al. (2025a). In that study, a formerly employed Nokia CML is used to obtain C_{nn} estimates by correcting the CML for the white noise floor in the received signal intensities using two proposed correction methods, a straightforward constant noise and a more advanced spectral noise method. In this study, we make use of both correction methods to obtain L_vE estimates from the estimated 30 min C_{nn} values with the same formerly employed Nokia CML. In general, all presented methods show that it is possible to obtain L_vE estimates using this Nokia CML. Moreover, conversion of the 30 min L_vE estimates to daily evaporation estimates keeps on average a similar bias.

5.1 Energy-balance method versus two-wavelength method

Similar to the C_{nn} estimates reported in van der Valk et al. (2025a), the spectral noise correction method outperforms the constant noise method for the L_vE estimates. As shown in van der Valk et al. (2025a), the spectral noise method mostly reduces the IQR in C_{nn} estimates, which is also reflected in our results. When using the two-wavelength method with the spectral noise method and free-convection scaling, the performance of the L_vE estimates is roughly comparable to the intercomparison between our reference in-

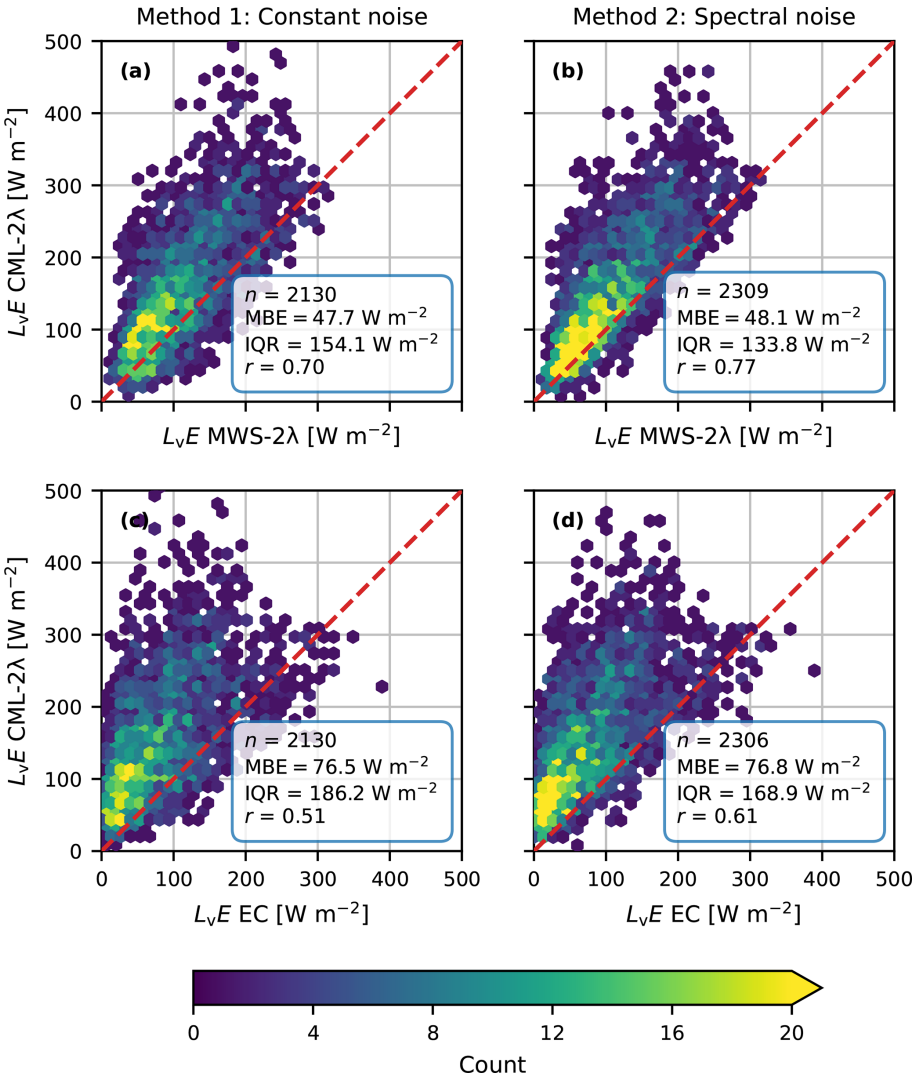


Figure 5. Comparison of 30 min L_vE estimates obtained with the Nokia CML using the two-wavelength method with the complete scaling for the entire study period, post-processed with the constant noise method **(a, c)** and spectral noise method **(b, d)** versus the MWS-2λ method **(a, b)** and the EC **(c, d)** estimates. The dashed red line is the 1 : 1 line.

struments, the MWS-2λ method and EC system. Using the complete scaling instead, the performance of the L_vE estimates decreases, due to the overestimation of C_{nn} after correction (van der Valk et al., 2025a). The MWS-2λ method estimates larger L_vE values than the EC system, similar to Meijninger et al. (2002, 2006) and Ward et al. (2015a), while the spread in our comparison of the reference instruments is similar to these studies, too.

However, the two-wavelength method can usually not be applied for an entire CML network, due to the absence of a LAS. To overcome this limitation, the EBM proposed by Leijnse et al. (2007b) can be used, which requires net radiation as additional constraint and assumes closure of the measured energy balance. The L_vE estimates of the EBM-OBS are most similar to the reference instruments. Surprisingly, this method even outperformed the two-wavelength method, which is traditionally used in scintillometry. However, this method largely overestimates H, which reduces the overall performance of the EBM-OBS. For the two-wavelength method, the performance of the H estimates is comparable to the L_vE estimates and also comparable to the intercomparison of our reference methods (as the LAS is the main contributor to the H estimates in the two-wavelength method).

Moreover, net radiation is not frequently measured either, which motivated us to consider a satellite-derived radiation product as well. In our case, we use the LSA SAF radiation products and assume that 10 % of the net radiation is used for the ground heat flux. Generally, the net radiation obtained from LSA SAF overestimates the measured net radiation at Cabauw, so that the sum of the turbulent heat fluxes is also overestimated. This underlines the bottleneck of this method, in which the performance of the used net radiation

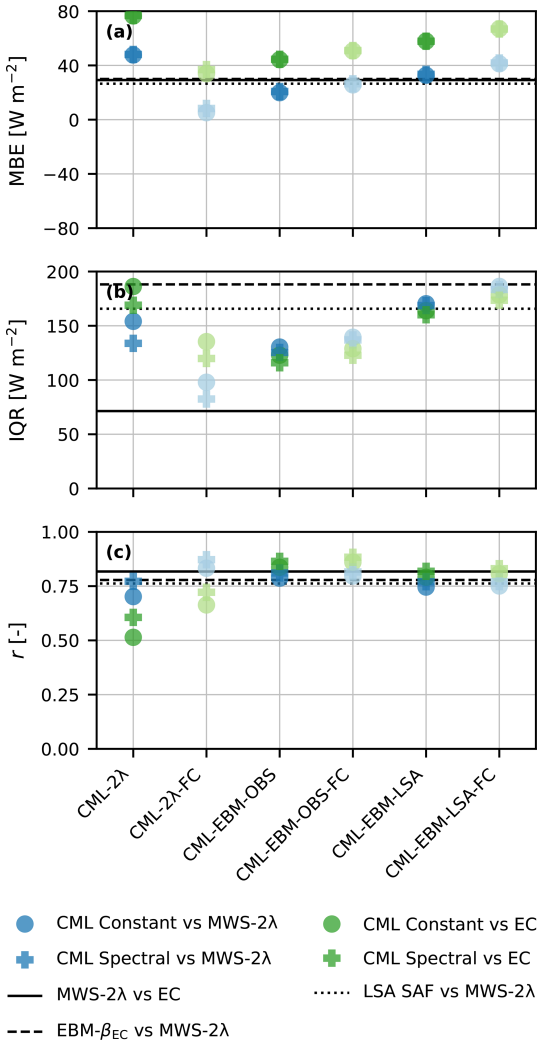


Figure 6. Statistical metrics per method and scaling to obtain L_vE estimates using the Nokia CML for both correction methods (shape) versus both reference instruments (color). The solid line indicates the statistical metrics of the reference instruments versus each other (Fig. 3). CML-2λ method uses the two-wavelength scintillation method with the CML and LAS, CML-EBM-OBS uses the measured energy balance method as constraint to infer the turbulent heat fluxes and CML-EBM-LSA uses the estimated net radiation by LSA SAF instead of the measured net radiation. The "FC"-suffix refers to the free-convection scaling. The dotted line shows the statistical metrics of a comparison between the L_vE estimates directly obtained from LSA SAF versus the MWS-2λ method. The dashed line represents L_vE estimates based on the measured available energy ($R_{net}-G$) and the Bowen ratio β obtained from the EC-system, i.e., $\frac{R_{net}-G}{1+\beta}$ versus the MWS-2λ method. The used Bowen ratio is a median value for the full data period (excluding nighttime intervals), as a means to obtain an objectively selected, representative Bowen ratio value to estimate L_vE from only net radiation measurements. We refer the reader to Appendix A for a complete overview of the used abbreviations.

product largely affects the performance of the turbulent heat fluxes, especially the MBE. For LSA SAF, Rains et al. (2024) finds over Europe an average underestimation of 9 W m^{-2}, with overall a relatively spatially homogeneous performance. However, in more complex environments the net radiation determination can be more difficult. Yet, the EBM-LSA does provide a decent estimate of L_vE, especially when considering it would allow to estimate L_vE using CMLs in places where other measurements are lacking. Other possibilities to obtain net radiation could be based on more basic meteorological measurements, such as suggested by Holtslag and Van Ulden (1983), but do require the use of multiple constants which depend on the local conditions.

Our results show the benefits of using CMLs to estimate L_vE, especially for the EBM-OBS. These EBM estimates show an improvement when comparing to L_vE estimates obtained from measured net radiation and a prescribed Bowen ratio, i.e., the median of the Bowen ratio measured by the EC over all used time intervals, predominantly by reducing the spread. Moreover, in comparison to L_vE estimates obtained from LSA SAF data product, the EBM-OBS shows an improvement, while EBM-LSA does not show any improvement in comparison to these LSA SAF L_vE estimates. Overall, this illustrates the potential of the EBM with measured net radiation, but also the dependence of this method on the quality of the measured net radiation estimates.

However, application of the EBM is not trivial in general, let alone over complex terrain, such as cities or forests. Typically, the observed energy balance does not close (Mauder et al., 2020), which is also the case for our field site (Kroon, 2004). For cities the addition of the anthropogenic heat flux as heat source for the turbulent heat fluxes (e.g., Oke et al., 2017) and the significant amount of heat storage (e.g., Sun et al., 2017) can complicate the application of the EBM (e.g., Harman and Belcher, 2006; Miao et al., 2012). These fluxes are added to the energy balance, so that the assumed energy balance for the EBM versions is not valid for every CML in cities. Moreover, the validity of the EBM also depends on the location of the CML, for example the mounting height, which affects the footprint of the CML to be on local scales, i.e., streets for cities, or more regional scales, i.e., city (or neighbourhood) scales.

5.2 MOST L_vE estimates versus free-convection

The complete MOST scaling requires temperature, humidity and horizontal wind speed measurements and estimates of the roughness length. To eliminate the dependency on horizontal wind speed and roughness length, we apply the free-convection scaling. These eliminated variables have a relatively large influence on the performance of the L_vE estimates, especially for large C_{nn} values, and thus L_vE (Leijnse et al., 2007b; Ward et al., 2014). Additionally, these variables can be relatively hard to measure in complex environments and would require a more elaborate setup. On the

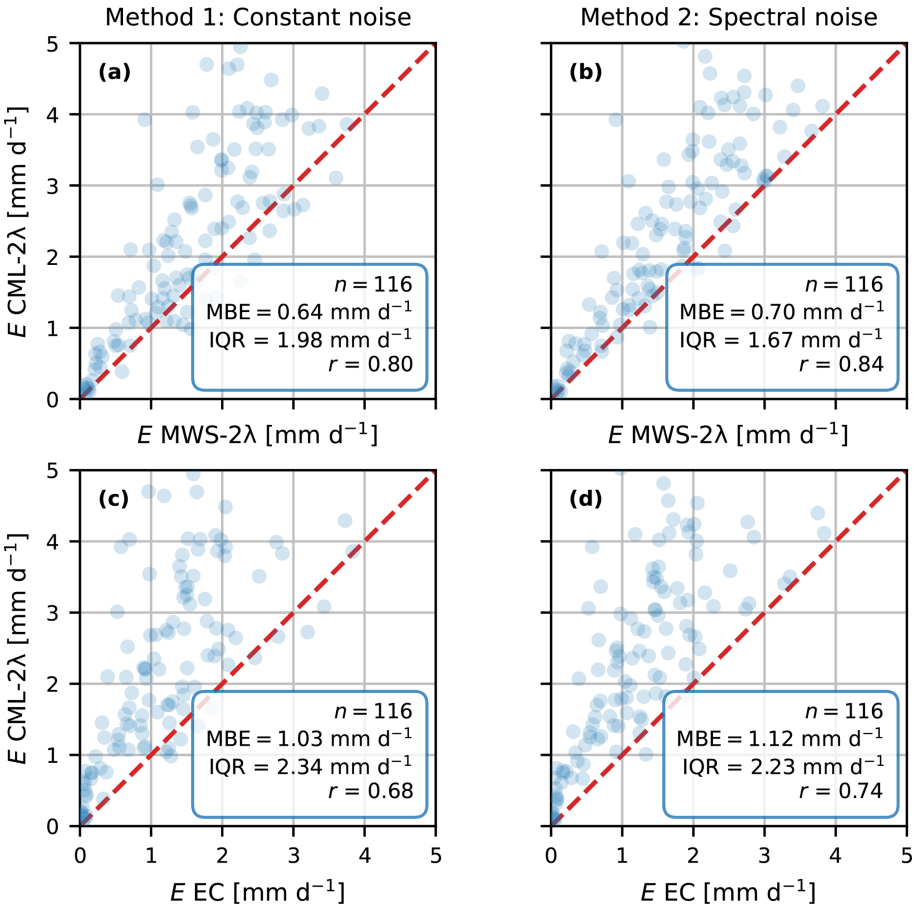


Figure 7. Comparison of daily E estimates obtained with the Nokia CML in combination with the LAS using the two-wavelength method for the entire study period, post-processed with the constant noise method **(a, c)** and spectral noise method **(b, d)** versus the MWS-2λ method **(a, b)** and the EC **(c, d)** estimates. The red line is the 1 : 1 line.

other hand, the use of free-convection scaling introduces an underestimation of the turbulent heat fluxes by assuming that turbulence is only buoyancy-driven and neglecting the shear-driven part, which is confirmed by our findings for the two-wavelength method, similar to Kohsiek (1982) and De Bruin et al. (1995). Moreover, typical mounting heights of CMLs are at least around 20–30 m above the surface, so that $-\frac{z}{L_{\mathrm{Ob}}}$ increases in comparison to our setup and the underestimation of the turbulent heat fluxes reduces. However, it must be noted that for the EBM versions, the use of free-convection causes an increase in the $L_{\mathrm{v}}E$ estimates and a reduction in H in comparison to the complete scaling. H reduces due to the strong relation with the free-convection wind scaling variable u_{fc} (Eq. 11), which decreases compared to the friction velocity u_*, so that $L_{\mathrm{v}}E$ has to increase as a consequence of the prescribed available energy that needs to be distributed among the two turbulent heat fluxes.

For both scaling methods information on r_{Tq} is required, in order to determine C_{TT} and C_{qq}. The value of r_{Tq} can be determined by using the bichromatic method proposed by Lüdi et al. (2005) or using an EC system or, alternatively, a value has to be assumed (although for flows following MOST, r_{Tq} has to be equal to one for two conservative scalars; Hill, 1989). The bichromatic method is not applicable to the Nokia CML, given the large amount of noise added to the signal. In our case, we assumed r_{Tq} to be equal to 0.8, following the recommendations of Ward et al. (2015b). Previous studies suggest r_{Tq} to be just below 1 during the day for many different types of surface (e.g., Kohsiek, 1982; Priestley and Hill, 1985; Andreas et al., 1998; Beyrich et al., 2005; Ward et al., 2015b), while an intercomparison of multiple studies by Andreas (1987) revealed a maximum around 0.8. Moreover, Ward et al. (2015b) reports a decrease in maximum r_{Tq} values for their setup during winter months towards approximately 0.5, while Leijnse et al. (2007b) report a relatively high sensitivity of $L_{\mathrm{v}}E$ estimates to r_{Tq} for low C_{nn} values. So, when assuming r_{Tq} values for application in CML networks a seasonally-dependent value could result in improved $L_{\mathrm{v}}E$ estimates, even though it should be noted that $L_{\mathrm{v}}E$ during winter months is relatively low. Overall, assuming that r_{Tq} equals 0.8 during the day seems a reasonable

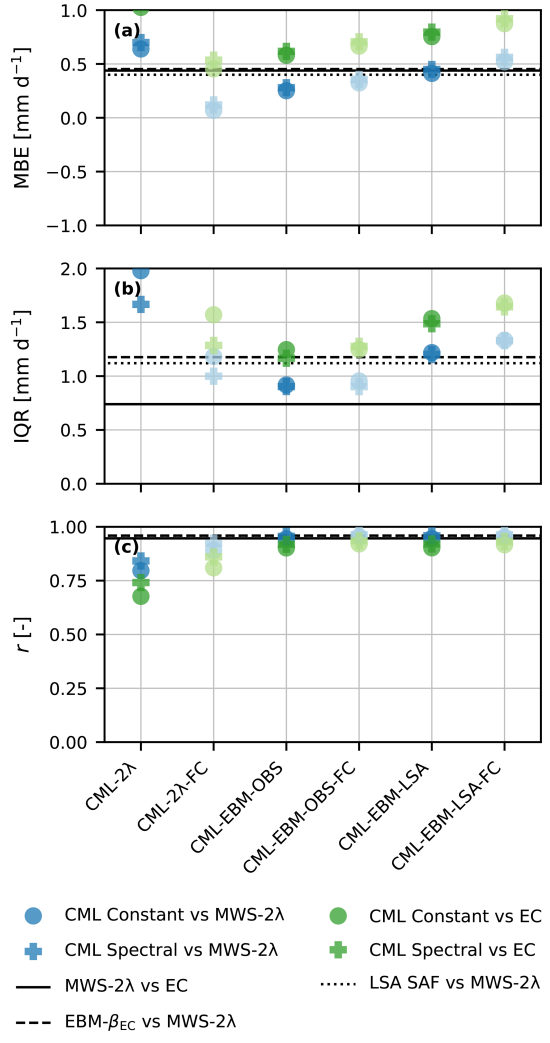


Figure 8. Statistical metrics per method and scaling to obtain daily E estimates using the Nokia CML for both correction methods (shape) versus both reference instruments (color). The solid line indicates the statistical metrics of the reference instruments versus each other (Fig. 3). CML-2λ method uses the two-wavelength scintillation method with the CML and LAS, CML-EBM-OBS uses the measured energy balance method as constraint to infer the turbulent heat fluxes and CML-EBM-LSA uses the estimated net radiation by LSA SAF instead of the measured net radiation. The "FC"-suffix refers to the free-convection scaling. The dotted line shows the statistical metrics of a comparison between the L_vE estimates directly obtained from LSA SAF versus the MWS-2λ method method. The dashed line represents L_vE estimates based on the measured available energy ($R_{net}-G$) and the Bowen ratio β obtained from the EC-system, i.e., $\frac{R_{net}-G}{1+\beta}$ versus the MWS-2λ method. The used Bowen ratio is a median value for the full data period (excluding nighttime intervals), as a means to obtain an objectively selected, representative Bowen ratio value to estimate L_vE from only net radiation measurements. We refer the reader to Appendix A for a complete overview of the used abbreviations.

estimate, especially when focusing on evaporation during the evaporation season.

5.3 Potential of CMLs to estimate L_vE

Extrapolation of our results to CML networks is not directly possible. Firstly, not all CML antennas modify the received signal intensity in the same manner. For example, in van der Valk et al. (2025a), we rejected a formerly employed Ericsson CML, due to the 0.5 dB power quantization by the antenna. Next to this quantization, CML data is typically not provided at 20 Hz, but either a minimum and maximum signal intensity value per 15 min time interval or an instantaneous value every second to minute. Also, other types of CML antennas might have different noise floors than the Nokia CML.

Secondly, we have tested our methods for Cabauw, the Netherlands, where the water table is managed and with relatively idealized conditions. For example, the Bowen ratio is relatively constant throughout the entire year. Generally, microwave scintillometry has proven itself as reliable method to estimate L_vE over different landscapes, such as heterogeneous farmlands (e.g., Meijninger et al., 2002, 2006; Beyrich et al., 2005; Xu et al., 2023), cities (Ward et al., 2015a). Also, in areas with a more complex topography, scintillometry has shown its value for estimating the turbulent heat fluxes, especially on larger-scales, such as over vineyards (Perelet et al., 2022) or hilly forests (Isabelle et al., 2019). For H, several studies, some only using an optical scintillometer, have shown the potential over heterogeneous farmland (e.g., Beyrich et al., 2002; Ezzahar et al., 2007), arid regions with sparse vegetation (e.g., Asanuma and Iemoto, 2007; Kleissl et al., 2009), and cities (e.g., Lagouarde et al., 2006; Lee et al., 2015). Yee et al. (2015) compares several scintillometers and methods and identifies the difficulty using the two-wavelength method and EBM for higher Bowen ratios. For microwave scintillometry in dryer environments, Wesely (1976), Moene (2003), Leijnse et al. (2007b) and Ward et al. (2015b) emphasize the importance of correctly estimating r_{Tq}. Moreover, at Bowen ratios around 2–3, C_{nn} at microwave wavelengths can theoretically approach zero (for $r_{Tq} = \pm 1$), due to the C_{Tq} term in Eq. (1) canceling the C_{TT} and C_{qq} terms (Hill et al., 1988; Leijnse et al., 2007b; Ward et al., 2013). If so, the actual C_{nn} values may drop below the detection limit of the scintillometer, due to the noise floor in receiving antennas. Our correction methods, in which we try to reduce the noise floor as much as possible, will likely also encounter difficulties for such Bowen ratios.

Future research to estimate evaporation using CMLs should focus on the typically employed sampling strategies of CMLs in communication networks, signal intensity modification by antennas and perhaps explore more opportunistic methods. Obtaining realistic C_{nn} from less frequently sampled signal intensities is complicated due to the undersampling of part of the turbulent power spectrum. Moreover, dif-

ferent noise floors in antennas or power quantization of the signal intensity also complicate C_{nn} computation.

6 Conclusions

In this study, we investigated the use of former CMLs to obtain 30 min L_vE and daily E estimates through scintillometry. We build on the results of van der Valk et al. (2025a), who obtained C_{nn} estimates by correcting a formerly employed Nokia CML for its noise floor. We computed L_vE estimates using the conventional two-wavelength method and a standalone method which prescribes the available energy for the turbulent heat fluxes based on net radiation, and compared these with an actual two-wavelength scintillometer setup and an EC system. Using the two-wavelength method, the performance of the turbulent heat flux estimates obtained with the free-convection scaling and spectral noise correction method is roughly comparable to the comparison between the reference MWS-2λ method and EC system, while application of the two-wavelength method combined with the complete scaling performs less well. In line with the C_{nn} estimates of van der Valk et al. (2025a), the spectral noise method reduces the spread in comparison to the constant method. For example, for the two-wavelength method using the complete scaling the IQR reduces from 154 to 134 W m^{-2} when comparing to the MWS-2λ method. However, application of the two-wavelength method is not possible for entire CML networks, as it would require installation of a LAS next to every CML.

As standalone alternative, the EBM versions require net radiation estimates as a constraint, so that this can be distributed over L_vE and H. The EBM using measured radiation seems to outperform the two-wavelength for the L_vE estimates, but the H estimates are worse. As an alternative to the radiation measurements, we used the LSA SAF radiation products to estimate the net radiation. The overestimation and uncertainty of the net radiation by LSA SAF in comparison to the measured net radiation is also reflected in the performance of our turbulent heat fluxes. The MBE and IQR of the latent heat flux estimates using the constant noise method and complete scaling increases from 20 to 33 W m^{-2} and from 130 to 170 W m^{-2} in comparison to the MWS-2λ method, respectively. Overall, this illustrates the dependence of the performance of the EBM versions on the quality of the net radiation data, while the assumption of closure of the measured energy balance is not always valid either. For example, over complex environments, such as cities or forest, additional uncertainties are introduced for this method.

The complete scaling of Monin-Obukhov requires temperature, humidity and wind speed measurements, and assumptions on the roughness length, next to C_{nn} (and the net radiation for the EBM). To eliminate the need for wind speed measurements and roughness length assumptions, we apply free-convection scaling instead of the complete scaling. This scaling neglects the shear-driven part of the turbulent heat fluxes, so that typically the fluxes tend to be underestimated. For our study, this results in an average reduction of the latent heat flux estimates of 40 W m^{-2} for the two-wavelength method with the spectral noise correction method. For the EBM versions, this underestimation is generally not applicable, since the method prescribes the amount of energy that needs to be distributed among the latent and sensible heat fluxes. For our experiment, this results in an increase in bias for the latent heat flux and a reduction in sensible heat flux estimates, with similar patterns emerging for the spread.

In general, our results illustrate the possibility to use CMLs as scintillometers. Also after aggregation of the 30 min L_vE estimates to daily E estimates, the performance remains comparable for almost all methods and days. This aggregation might be particularly interesting for hydrological applications, for example on spatial scales of catchments, which could be combined with the possibility to monitor rainfall using the same CMLs. However, our results also illustrate that the accuracy of the L_vE estimates using CML networks will largely depend on the quality of the radiation estimates. The quality of widely available radiation data, such as LSA SAF, seems too low for our purposes, and needs to be addressed in future research. Additionally, attempts to estimate evaporation using different CML types and employed sampling strategies of networks would be required, while also the performance of the proposed methods and scalings need to be tested in different climatic settings. If these issues would be addressed, CMLs could show a large potential to be used to estimate evaporation, especially considering the existing infrastructure which is also present on locations where other observations are lacking.

Appendix A: Abbreviation list

Table A1. List of used abbreviations.

Abbreviation	Meaning
CML	Commercial Microwave Link
CML-2λ	Two-wavelength method using the commercial microwave link and large-aperture scintillometer applied with Monin-Obukhov similarity theory
CML-2λ-FC	Two-wavelength method to estimate the turbulent heat fluxes using the commercial microwave link and large-aperture scintillometer applied with free convection scaling
CML-EBM-OBS	Energy-balance method to estimate the turbulent heat fluxes using the commercial microwave link and observed net radiation and ground heat flux applied with Monin-Obukhov similarity theory
CML-EBM-OBS-FC	Energy-balance method to estimate the turbulent heat fluxes using the commercial microwave link and observed net radiation and ground heat flux applied with free convection scaling
CML-EBM-LSA	Energy-balance method to estimate the turbulent heat fluxes using the commercial microwave link and estimated net radiation by Satellite Application Facility on Land Surface Analysis data products applied with Monin-Obukhov similarity theory
CML-EBM-LSA-FC	Energy-balance method to estimate the turbulent heat fluxes using the commercial microwave link and estimated net radiation by Satellite Application Facility on Land Surface Analysis data products with free convection scaling
EBM-β_{EC}	Energy-balance method to estimate the turbulent heat fluxes using measured net radiation and median Bowen ratio, measured by the eddy-covariance system
EC	Eddy-covariance system
LAS	Large-Aperture Scintillometer
LSA SAF	Satellite Application Facility on Land Surface Analysis
MBE	Mean Bias Error
MWS	Microwave Scintillometer
MWS-2λ	Two-wavelength method to estimate the turbulent heat fluxes using the microwave scintillometer and large-aperture scintillometer applied with Monin-Obukhov similarity theory
r	Pearson's correlation coefficient

Appendix B: Net radiation LSA SAF versus measurements

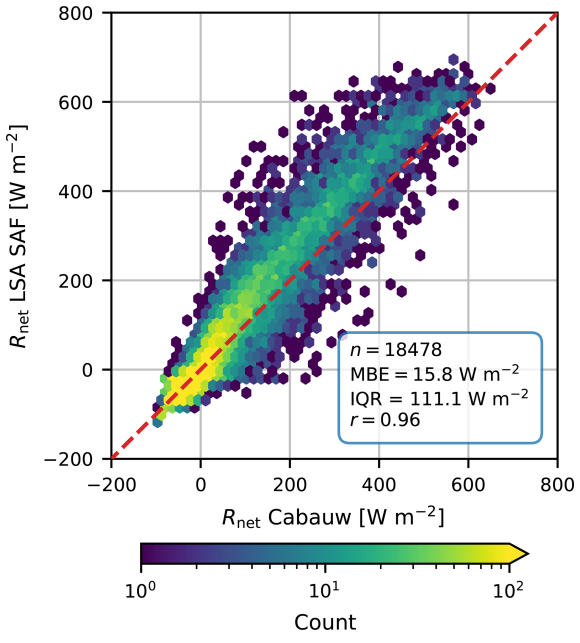


Figure B1. Comparison of 30 min R_{net} estimates using LSA SAF versus the net radiation measured at Cabauw for our data period.

Appendix C: Statistics H

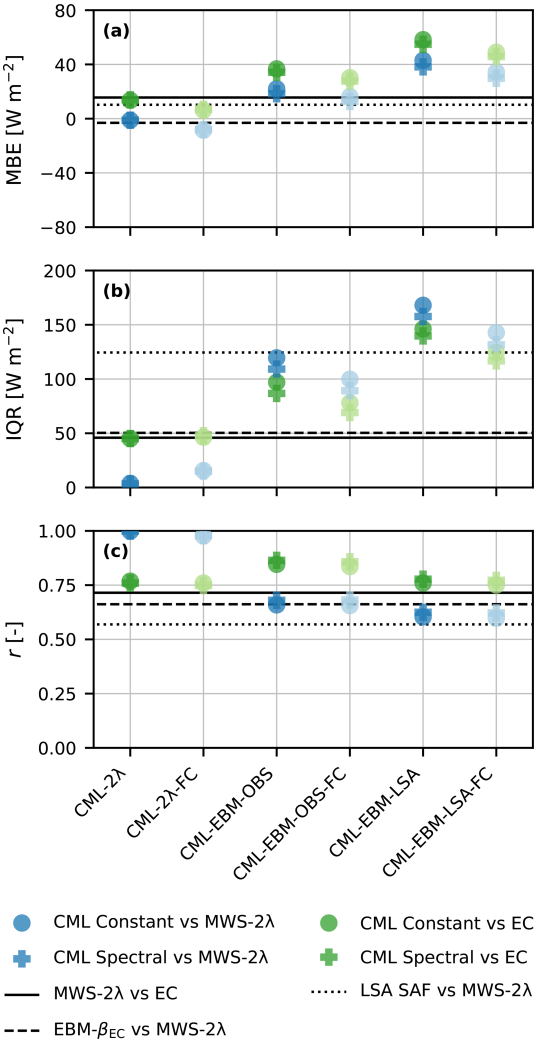


Figure C1. Statistical metrics per method to obtain H estimates using the Nokia CML for both correction methods (shape) versus both reference instruments (color). The solid line indicates the statistical metrics of the reference instruments versus each other. CML-2λ method uses the two-wavelength scintillation method with the CML and LAS, CML-EBM-OBS uses the measured energy balance method as constraint to infer the turbulent heat fluxes and CML-EBM-LSA uses the estimated net radiation by LSA SAF instead of the measured net radiation. The "FC"-suffix refers to the free-convection scaling. The dotted line shows the statistical metrics of a comparison between the H estimates directly obtained from LSA SAF versus the MWS-2λ method. The dashed line represents H estimates based on the measured available energy ($R_{net} - G$) and the Bowen ratio β obtained from the EC-system, i.e., $\frac{\beta(R_{net}-G)}{1+\beta}$ versus the MWS-2λ. The used Bowen ratio is a median value for the full data period (excluding nighttime intervals), as a means to obtain an objectively selected, representative Bowen ratio value to estimate H from only net radiation measurements. We refer the reader to Appendix A for a complete overview of the used abbreviations.

Code and data availability. The MWS and CML data can be found at https://doi.org/10.4121/247d47b7-2ea5-4e93-bffb-67620a66525c (van der Valk et al., 2024). KNMI data can be dowloaded from https://dataplatform.knmi.nl/ (KNMI Data Platform, 2024). For the code used to perform the analysis and create the figures, see https://github.com/LDvdValk/Python_scripts_vanderValketal2025.git (last access: 4 August 2025; DOI: https://doi.org/10.5281/zenodo.16737579, van der Valk et al., 2025b).

Supplement. The supplement related to this article is available online at https://doi.org/10.5194/hess-29-6589-2025-supplement.

Author contributions. LDvdV carried out the research under the supervision of OKH, MCG, RWH, and RU. LDvdV prepared the manuscript, with contributions from all co-authors.

Competing interests. At least one of the (co-)authors is a member of the editorial board of *Hydrology and Earth System Sciences*. The peer-review process was guided by an independent editor, and the authors also have no other competing interests to declare.

Disclaimer. Publisher's note: Copernicus Publications remains neutral with regard to jurisdictional claims made in the text, published maps, institutional affiliations, or any other geographical representation in this paper. While Copernicus Publications makes every effort to include appropriate place names, the final responsibility lies with the authors. Views expressed in the text are those of the authors and do not necessarily reflect the views of the publisher.

Financial support. This manuscript has been accomplished by using (data generated in) the Ruisdael Observatory, a scientific research infrastructure which is (partly) financed by the Dutch Research Council (NWO, grant number 184.034.015).

Review statement. This paper was edited by Bob Su and reviewed by Prajwal Khanal and two anonymous referees.

References

ABI research: Wireless Backhaul Evolution Delivering Next-Generation Connectivity, https://www.gsma.com/spectrum/wp-content/uploads/2022/04/wireless-backhaul-spectrum.pdf (last access: 30 January 2024), 2021.

Andreas, E. L.: On the Kolmogorov Constants for the Temperature-Humidity Cospectrum and the Refractive Index Spectrum, Journal of Atmospheric Sciences, 44, 2399–2406, https://doi.org/10.1175/1520-0469(1987)044<2399:OTKCFT>2.0.CO;2, 1987.

Andreas, E. L., Hill, R. J., Gosz, J. R., Moore, D. I., Otto, W. D., and Sarma, A. D.: Statistics of Surface-Layer Turbulence Over Terrain with Metre-Scale Heterogeneity, Boundary-Layer Meteorology, 86, 379–408, https://doi.org/10.1023/A:1000609131683, 1998.

Asanuma, J. and Iemoto, K.: Measurements of regional sensible heat flux over Mongolian grassland using large aperture scintillometer, Journal of Hydrology, 333, 58–67, https://doi.org/10.1016/j.jhydrol.2006.07.031, 2007.

Beyrich, F., Richter, S. H., Weisensee, U., Kohsiek, W., Lohse, H., de Bruin, H. A. R., Foken, T., Göckede, M., Berger, F., Vogt, R., and Batchvarova, E.: Experimental determination of turbulent fluxes over the heterogeneous LITFASS area: Selected results from the LITFASS-98 experiment, Theoretical and Applied Climatology, 73, 19–34, https://doi.org/10.1007/s00704-002-0691-7, 2002.

Beyrich, F., Kouznetsov, R. D., Leps, J.-P., Lüdi, A., Meijninger, W. M., and Weisensee, U.: Structure parameters for temperature and humidity from simultaneous eddy-covariance and scintillometer measurements, Meteorologische Zeitschrift, 14, 641–649, https://doi.org/10.1127/0941-2948/2005/0064, 2005.

Bosveld, F. C., Baas, P., Beljaars, A. C. M., Holtslag, A. A. M., de Arellano, J. V.-G., and van de Wiel, B. J. H.: Fifty Years of Atmospheric Boundary-Layer Research at Cabauw Serving Weather, Air Quality and Climate, Boundary-Layer Meteorology, 177, 583–612, https://doi.org/10.1007/s10546-020-00541-w, 2020.

Brauer, C. C., Torfs, P. J. J. F., Teuling, A. J., and Uijlenhoet, R.: The Wageningen Lowland Runoff Simulator (WALRUS): application to the Hupsel Brook catchment and the Cabauw polder, Hydrol. Earth Syst. Sci., 18, 4007–4028, https://doi.org/10.5194/hess-18-4007-2014, 2014.

Brutsaert, W.: Evaporation into the atmosphere: theory, history and applications, Springer Science & Business Media, ISBN 978-90-277-1247-9, 1982.

De Bruin, H. A., Van den Hurk, B., and Kohsiek, W.: The scintillation method tested over a dry vineyard area, Boundary-Layer Meteorology, 76, 25–40, 1995.

EUMETSAT: LSA SAF, https://lsa-saf.eumetsat.int/en/ (last access: 28 January 2025), 2025.

Ezzahar, J., Chehbouni, A., Hoedjes, J., Er-Raki, S., Chehbouni, A., Boulet, G., Bonnefond, J.-M., and De Bruin, H.: The use of the scintillation technique for monitoring seasonal water consumption of olive orchards in a semi-arid region, Agricultural Water Management, 89, 173–184, https://doi.org/10.1016/j.agwat.2006.12.015, 2007.

Foken, T.: Springer handbook of atmospheric measurements, https://doi.org/10.1007/978-3-030-52171-4, 2021.

Green, A., Astill, M., McAneney, K., and Nieveen, J.: Path-averaged surface fluxes determined from infrared and microwave scintillometers, Agricultural and Forest Meteorology, 109, 233–247, https://doi.org/10.1016/S0168-1923(01)00262-3, 2001.

Harman, I. N. and Belcher, S. E.: The surface energy balance and boundary layer over urban street canyons, Quarterly Journal of the Royal Meteorological Society, 132, 2749–2768, https://doi.org/10.1256/qj.05.185, 2006.

Hill, R. J.: Implications of Monin–Obukhov Similarity Theory for Scalar Quantities, Journal of Atmospheric Sciences, 46, 2236–2244, https://doi.org/10.1175/1520-0469(1989)046<2236:IOMSTF>2.0.CO;2, 1989.

Hill, R. J.: Algorithms for obtaining atmospheric surface-layer fluxes from scintillation measurements, Journal of Atmospheric and Oceanic Technology, 14, 456–467, https://doi.org/10.1175/1520-0426(1997)014<0456:AFOASL>2.0.CO;2, 1997.

Hill, R. J., Bohlander, R. A., Clifford, S. F., McMillan, R. W., Priestly, J. T., and Schoenfeld, W. P.: Turbulence-induced millimeter-wave scintillation compared with micrometeorological measurements, IEEE Transactions on Geoscience and Remote Sensing, 26, 330–342, https://doi.org/10.1109/36.3035, 1988.

Holtslag, A. A. M. and Van Ulden, A. P.: A Simple Scheme for Daytime Estimates of the Surface Fluxes from Routine Weather Data, Journal of Applied Meteorology and Climatology, 22, 517–529, https://doi.org/10.1175/1520-0450(1983)022<0517:ASSFDE>2.0.CO;2, 1983.

Isabelle, P.-E., Nadeau, D. F., Perelet, A. O., Pardyjak, E. R., Rousseau, A. N., and Anctil, F.: Application and Evaluation of a Two-Wavelength Scintillometry System for Operation in a Complex Shallow Boreal-Forested Valley, Boundary-Layer Meteorology, 174, 341–370, https://doi.org/10.1007/s10546-019-00488-7, 2019.

Kleissl, J., Hong, S.-H., and Hendrickx, J. M. H.: New Mexico Scintillometer Network: Supporting Remote Sensing and Hydrologic and Meteorological Models, Bulletin of the American Meteorological Society, 90, 207–218, https://doi.org/10.1175/2008BAMS2480.1, 2009.

KNMI Data Platform: KNMI Data Platform, https://dataplatform.knmi.nl/, last access: 9 October 2024.

Kohsiek, W.: Measuring C_T^2, C_Q^2 and C_{TQ} in the unstable surface layer, and relations to the vertical fluxes of heat and moisture, Boundary-Layer Meteorology, 24, 89–107, https://doi.org/10.1007/BF00121802, 1982.

Kooijmans, L. M. J. and Hartogensis, O. K.: Surface-layer similarity functions for dissipation rate and structure parameters of temperature and humidity based on eleven field experiments, Boundary-Layer Meteorology, 160, 501–527, https://doi.org/10.1007/s10546-016-0152-y, 2016.

Kroon, P.: De sluiting van de oppervlakte energiebalans in Cabauw gedurende TEBEX (1995–1996), Tech. rep., KNMI, https://www.knmi.nl/kennis-en-datacentrum/publicatie/de-sluiting-van-de-oppervlakte-energiebalans-in-cabauw-gedurende-tebex-1995-1996 (last access: 30 June 2025), 2004.

Lagouarde, J. P., Irvine, M., Bonnefond, J. M., Grimmond, C., Long, N., Oke, T., Salmond, J., and Offerle, B.: Monitoring the sensible heat flux over urban areas using large aperture scintillometry: case study of Marseille city during the ESCOMPTE experiment, Boundary-Layer Meteorology, 118, 449–476, https://doi.org/10.1007/s10546-005-9001-0, 2006.

Lee, S.-H., Lee, J.-H., and Kim, B.-Y.: Estimation of turbulent sensible heat and momentum fluxes over a heterogeneous urban area using a large aperture scintillometer, Advances in Atmospheric Sciences, 32, 1092–1105, https://doi.org/10.1007/s00376-015-4236-2, 2015.

Leijnse, H., Uijlenhoet, R., and Stricker, J. N. M.: Rainfall measurement using radio links from cellular communication networks, Water Resources Research, 43, https://doi.org/10.1029/2006wr005631, 2007a.

Leijnse, H., Uijlenhoet, R., and Stricker, J. N. M.: Hydrometeorological application of a microwave link: 1. Evaporation, Water Resources Research, 43, https://doi.org/10.1029/2006wr004988, 2007b.

Lüdi, A., Beyrich, F., and Mätzler, C.: Determination of the Turbulent Temperature–Humidity Correlation from Scintillometric Measurements, Boundary-Layer Meteorology, 117, 525–550, https://doi.org/10.1007/s10546-005-1751-1, 2005.

Maes, W. H. and Steppe, K.: Estimating evapotranspiration and drought stress with ground-based thermal remote sensing in agriculture: a review, J. Exp. Bot., 63, 4671–712, https://doi.org/10.1093/jxb/ers165, 2012.

Mauder, M., Foken, T., and Cuxart, J.: Surface-Energy-Balance Closure over Land: A Review, Boundary-Layer Meteorology, 177, 395–426, https://doi.org/10.1007/s10546-020-00529-6, 2020.

Meijninger, W., Green, A., Hartogensis, O., Kohsiek, W., Hoedjes, J., Zuurbier, R., and De Bruin, H.: Determination of area-averaged water vapour fluxes with large aperture and radio wave scintillometers over a heterogeneous surface–Flevoland field experiment, Boundary-Layer Meteorology, 105, 63–83, https://doi.org/10.1023/A:1019683616097, 2002.

Meijninger, W. M. L., Beyrich, F., Lüdi, A., Kohsiek, W., and Bruin, H. A. R. D.: Scintillometer-Based Turbulent Fluxes of Sensible and Latent Heat Over a Heterogeneous Land Surface – A Contribution to Litfass-2003, Boundary-Layer Meteorology, 121, 89–110, https://doi.org/10.1007/s10546-005-9022-8, 2006.

Messer, H., Zinevich, A., and Alpert, P.: Environmental monitoring by wireless communication networks, Science, 312, 713, https://doi.org/10.1126/science.1120034, 2006.

Miao, S., Dou, J., Chen, F., Li, J., and Li, A.: Analysis of observations on the urban surface energy balance in Beijing, Science China Earth Sciences, 55, 1881–1890, https://doi.org/10.1007/s11430-012-4411-6, 2012.

Moene, A. F.: Effects of water vapour on the structure parameter of the refractive index for near-infrared radiation, Boundary-Layer Meteorology, 107, 635–653, https://doi.org/10.1023/A:1022807617073, 2003.

Monin, A. S. and Obukhov, A. M.: Basic laws of turbulent mixing in the surface layer of the atmosphere, Contrib. Geophys. Inst. Acad. Sci. USSR, 151, 163–187, 1954.

Moonen, R.: Performance of long-path optical-microwave Scintillometry, Master's thesis, Wageningen University, https://edepot.wur.nl/703856 (last access: 18 November 2025), 2021.

Oke, T. R., Mills, G., Christen, A., and Voogt, J. A.: Energy Balance, Cambridge University Press, Cambridge, 156–196, ISBN 9781139016476, https://doi.org/10.1017/9781139016476.007, 2017.

Pallandt, M. M. T. A., Kumar, J., Mauritz, M., Schuur, E. A. G., Virkkala, A.-M., Celis, G., Hoffman, F. M., and Göckede, M.: Representativeness assessment of the pan-Arctic eddy covariance site network and optimized future enhancements, Biogeosciences, 19, 559–583, https://doi.org/10.5194/bg-19-559-2022, 2022.

Perelet, A. O., Ward, H. C., Stoll, R., Mahaffee, W. F., and Pardyjak, E. R.: Quantifying Turbulence Heterogeneity in a Vineyard Using Eddy-Covariance and Scintillometer Measurements, Boundary-Layer Meteorology, 184, 479–504, https://doi.org/10.1007/s10546-022-00714-9, 2022.

Priestley, J. T. and Hill, R. J.: Measuring High-Frequency Humidity, Temperature and Radio Refractive Index in the Surface Layer, Journal of Atmospheric and Oceanic Technology, 2, 233–251, https://doi.org/10.1175/1520-0426(1985)002<0233:MHFHTA>2.0.CO;2, 1985.

Rains, D., Trigo, I., Dutra, E., Ermida, S., Ghent, D., Hulsman, P., Gómez-Dans, J., and Miralles, D. G.: High-resolution (1 km) all-sky net radiation over Europe enabled by the merging of land surface temperature retrievals from geostationary and polar-orbiting satellites, Earth Syst. Sci. Data, 16, 567–593, https://doi.org/10.5194/essd-16-567-2024, 2024.

Sun, T., Wang, Z.-H., Oechel, W. C., and Grimmond, S.: The Analytical Objective Hysteresis Model (AnOHM v1.0): methodology to determine bulk storage heat flux coefficients, Geosci. Model Dev., 10, 2875–2890, https://doi.org/10.5194/gmd-10-2875-2017, 2017.

van der Valk, L. D., Hartogensis, O. K., Coenders-Gerrits, M., Hut, R. W., Walraven, B., and Uijlenhoet, R.: Dataset: Use of commercial microwave links as scintillometers, 4TU.ResearchData [data set], https://doi.org/10.4121/247d47b7-2ea5-4e93-bffb-67620a66525c, 2024.

van der Valk, L. D., Hartogensis, O. K., Coenders-Gerrits, M., Hut, R. W., Walraven, B., and Uijlenhoet, R.: Use of commercial microwave links as scintillometers: potential and limitations towards evaporation estimation, Atmos. Meas. Tech., 18, 6143–6165, https://doi.org/10.5194/amt-18-6143-2025, 2025a.

van der Valk, L. D., Hartogensis, O. K., Coenders-Gerrits, M., Hut, R. W., and Uijlenhoet, R.: Use of commercial microwave links as scintillometers (v1.0.0), Zenodo [code], https://doi.org/10.5281/zenodo.16737579, 2025b.

Verkaik, J. W. and Holtslag, A. A. M.: Wind profiles, momentum fluxes and roughness lengths at Cabauw revisited, Boundary-Layer Meteorology, 122, 701–719, https://doi.org/10.1007/s10546-006-9121-1, 2007.

Villarreal, S. and Vargas, R.: Representativeness of FLUXNET sites across Latin America, Journal of Geophysical Research: Biogeosciences, 126, https://doi.org/10.1029/2020jg006090, 2021.

Ward, H. C.: Scintillometry in urban and complex environments: a review, Measurement Science and Technology, 28, https://doi.org/10.1088/1361-6501/aa5e85, 2017.

Ward, H. C., Evans, J. G., Hartogensis, O. K., Moene, A. F., De Bruin, H. A. R., and Grimmond, C. S. B.: A critical revision of the estimation of the latent heat flux from two-wavelength scintillometry, Quarterly Journal of the Royal Meteorological Society, 139, 1912–1922, https://doi.org/10.1002/qj.2076, 2013.

Ward, H. C., Evans, J. G., and Grimmond, C. S. B.: Multi-Scale Sensible Heat Fluxes in the Suburban Environment from Large-Aperture Scintillometry and Eddy Covariance, Boundary-Layer Meteorology, 152, 65–89, https://doi.org/10.1007/s10546-014-9916-4, 2014.

Ward, H. C., Evans, J. G., and Grimmond, C. S. B.: Infrared and millimetre-wave scintillometry in the suburban environment – Part 2: Large-area sensible and latent heat fluxes, Atmos. Meas. Tech., 8, 1407–1424, https://doi.org/10.5194/amt-8-1407-2015, 2015a.

Ward, H. C., Evans, J. G., Grimmond, C. S. B., and Bradford, J.: Infrared and millimetre-wave scintillometry in the suburban environment – Part 1: Structure parameters, Atmos. Meas. Tech., 8, 1385–1405, https://doi.org/10.5194/amt-8-1385-2015, 2015b.

Wesely, M. L.: The combined effect of temperature and humidity fluctuations on refractive index, Journal of Applied Meteorology, 43–49, https://doi.org/10.1175/1520-0450(1976)015<0043:TCEOTA>2.0.CO;2, 1976.

Wyngaard, J. C., Coté, O. R., and Izumi, Y.: Local Free Convection, Similarity, and the Budgets of Shear Stress and Heat Flux, Journal of Atmospheric Sciences, 28, 1171–1182, https://doi.org/10.1175/1520-0469(1971)028<1171:LFCSAT>2.0.CO;2, 1971a.

Wyngaard, J. C., Izumi, Y., and Collins, S. A.: Behavior of the refractive-index-structure parameter near the ground, Journal of the Optical Society of America, 61, 1646–1650, https://doi.org/10.1364/JOSA.61.001646, 1971b.

Xu, F., Wang, W., Huang, C., Wang, J., Ren, Z., Feng, J., Dong, L., Zhang, Y., and Kang, J.: Turbulent fluxes at kilometer scale determined by optical-microwave scintillometry in a heterogeneous oasis cropland of the Heihe River Basin, Agricultural and Forest Meteorology, 339, 109544, https://doi.org/10.1016/j.agrformet.2023.109544, 2023.

Yee, M. S., Pauwels, V. R. N., Daly, E., Beringer, J., Rüdiger, C., McCabe, M. F., and Walker, J. P.: A comparison of optical and microwave scintillometers with eddy covariance derived surface heat fluxes, Agricultural and Forest Meteorology, 213, 226–239, https://doi.org/10.1016/j.agrformet.2015.07.004, 2015.

Zhang, K., Kimball, J. S., and Running, S. W.: A review of remote sensing based actual evapotranspiration estimation, Wiley interdisciplinary reviews: Water, 3, 834–853, https://doi.org/10.1002/wat2.1168, 2016.